Article:
Laurent, H orcid.org/0000-0002-8925-4773, Soper, AK and Dougan, L orcid.org/0000-0002-2620-5827 (2020) Trimethylamine N-oxide (TMAO) resists the compression of water structure by magnesium perchlorate: terrestrial kosmotrope vs. Martian chaotrope. Physical Chemistry Chemical Physics, 22 (9). pp. 4924-4937. ISSN 1463-9076

https://doi.org/10.1039/c9cp06324b

Trimethylamine N-oxide (TMAO) Resists The Compression of Water Structure by Magnesium Perchlorate : Terrestrial Kosmotrope vs Martian Chaotrope

Harrison Laurent[1], Alan Soper[2], Lorna Dougan[1,3]

[1]Department of Physics and Astronomy, University of Leeds, Leeds, UK; [2]ISIS Facility, STFC Rutherford Appleton Laboratory, Didcot, UK; [3]Astbury Centre for Structural and Molecular Biology, University of Leeds, Leeds, UK

ORCiD:

Harrison Laurent: 0000-0002-8925-4773

Lorna Dougan: 0000-0002-2620-5827

1. Abstract

The presence of magnesium perchlorate ($Mg(ClO_4)_2$) as the dominating ionic compound in the Martian regolith and the recent discovery of a subsurface lake on Mars suggests that beneath the Martian surface may lie an aqueous environment suitable for life, rich in chaotropic ions. Closer to Earth, terrestrial organisms use osmolytes, such as trimethylamine N-oxide (TMAO), to overcome the biologically damaging effects of pressure. While previous studies have revealed that $Mg(ClO_4)_2$ acts to modify water structure as if it has been pressurized, little is known about the competing effects of chaotropes and kosmotropes. Therefore the question here is whether TMAO can help to preserve the hydrogen bond network of water against the pressurising effect of $Mg(ClO_4)_2$? We address this question using neutron scattering, computational modelling using Empirical Potential Structure Refinement (EPSR) analysis, and a new approach to quantifying hydrogen bond conformations and energies. We find that the addition of 1.0 M TMAO to 0.2 M $Mg(ClO_4)_2$ or 2.7 M $Mg(ClO_4)_2$ is capable of partially restoring the hydrogen bond network of water, and the fraction of water molecules in conformations associated with hydrogen bond switching. This suggests that terrestrial protecting osmolytes could provide a protective mechanism to the extremes found in Martian environments for biological systems.

2. Introduction

Liquid water lies at the most fundamental level of life as we know it, and yet despite extensive research there is no conclusive theory which accurately explains its host of unusual, and sometimes counterintuitive, properties(1–5). Its maximum density at 4°C, unusually high heat capacity and low compressibility are examples of these. The response of the hydrogen bonded loosely packed network of liquid water to solutes such as ions and amphiphilic molecules has been examined in depth by techniques such as Raman(6,7), IR spectroscopy(8–14), molecular dynamics simulations(15–22), NMR(23), X-ray diffraction(24,25) and neutron diffraction(26–33), which has allowed us to visualise structure making (kosmotropic) and structure breaking (chaotropic) effects. One of the most striking results is the modification to water structure as a result of ion addition, which is often similar to that of pure water under pressure(29,30).

Neutron diffraction combined with empirical potential structure refinement (EPSR) showed that at a concentration of 44 wt% (2.7 M) and 298 K, the highly chaotropic salt $Mg(ClO_4)_2$ is capable of perturbing the structure of water in the same manner as an external pressure of 3 GPa(30). This $Mg(ClO_4)_2$ induced perturbation of water structure is currently of particular interest due to the recent

discovery of periods of flowing surface water on Mars(34) and the presence of subsurface liquid water in the form of a lake(35), which may be one of many. $Mg(ClO_4)_2$ is present in surprisingly high quantities (Mg^{2+} at 3.3×10^{-3} m and ClO_4^- at 2.4×10^{-3} m where the concentrations are given in molality), dominating the ionic makeup of the Martian regolith at the Phoenix lander site(36,37). As the landing site in the Vastitas Borealis plains was chosen to study the history of water on Mars this striking result allows us to speculate that $Mg(ClO_4)_2$ may also be present in the subsurface lakes. This would provide an aqueous environment in a similar geographical location to Lake Vostok(38) or Lake Whillans(39) on Earth, with an interesting ionic composition, similar to the high salt concentration environments on Earth such as salt lakes and solar salterns(40), that would be protected from the combined bacteriocidal effects of $Mg(ClO_4)_2$ and UV radiation present at the surface(41).

We have previously shown that hydrogen bonding between amino acids is reduced but can still persist even in concentrated $Mg(ClO_4)_2$(42). Many terrestrial organisms use osmolytes as stabilising agents against the detrimental effects of their biochemistry, such as urea in the cells of sharks and rays(43), or their environment, such as extreme pressures experienced by snailfish(44). A commonly used osmolyte and powerful protein stabilising agent is trimethylamine N-oxide (TMAO). TMAO has already been shown to protect proteins against denaturation against a range of agents including urea(45,46) and pressure(47,48), as well as enhancing hydrogen bonding in bulk water(49–51). This motivates us to ask the question: can TMAO help to preserve the hydrogen bond network of water against the pressurising effect of $Mg(ClO_4)_2$? To address this, we have examined a solution at two $Mg(ClO_4)_2$ concentrations: the previously studied concentration of 44 wt% (2.7 M), and a lower concentration of 0.2 M.

This lower concentration was chosen because in order to study the counteracting ability of TMAO to the pressurising effect of $Mg(ClO_4)_2$ it is sensible to try and study an $Mg(ClO_4)_2$ concentration that perturbs water structure in such a way that it is noticeable through neutron scattering, but not so extreme that any resisting effects caused by TMAO would overwhelmed. We therefore wish to choose a concentration that is equivalent to a pressurising effect of 2-3 kbar. As there is no direct measure of the pressurising effect of $Mg(ClO_4)_2$ as a function of concentration we must attempt to estimate one using available published data (Figures 1 and 2). A property of $Mg(ClO_4)_2$ solutions that *has* been studied in detail is the melting temperature by Pestova et al.(52), which shows a roughly exponential dependence as a function of concentration measured in molality until a concentration corresponding to 44 wt% and is reproduced in figure 1(a). If one assumes that the density of solution is proportional to the wt% of the solute, as is the case in other salt solutions(53), and uses the experimental density of the 2.7 M $Mg(ClO_4)_2$ solution measured in this work, it is possible to convert the molality concentration in Pestova et al. to a molarity concentration. If one also assumes that the change in melting temperature serves as a good indication of the change in water structure of the system, then the induced pressure should be proportional to the change in melting temperature. Using the information that 2.7 M is equivalent to an external pressure of 3 GPa(30) (30 kbar) (point circled in Figure 1(b)), it is then possible to relate all the melting temperature data points in Pestova et al. to an equivalent induced pressure, and fit the data to an exponential growth. This fit is shown in Figure 1(b). This reveals that a concentration of 0.2 M $Mg(ClO_4)_2$ may result in an induced pressure of 2.2 kbar. It is important to note that because the melting temperature data does not extrapolate to 0^oC at 0 concentration, the induced pressure as a function of concentration does not extrapolate to atmospheric pressure at 0 concentration either. However as this is merely an estimate drawn from limited data, it should be a reasonable approximation for our purposes.

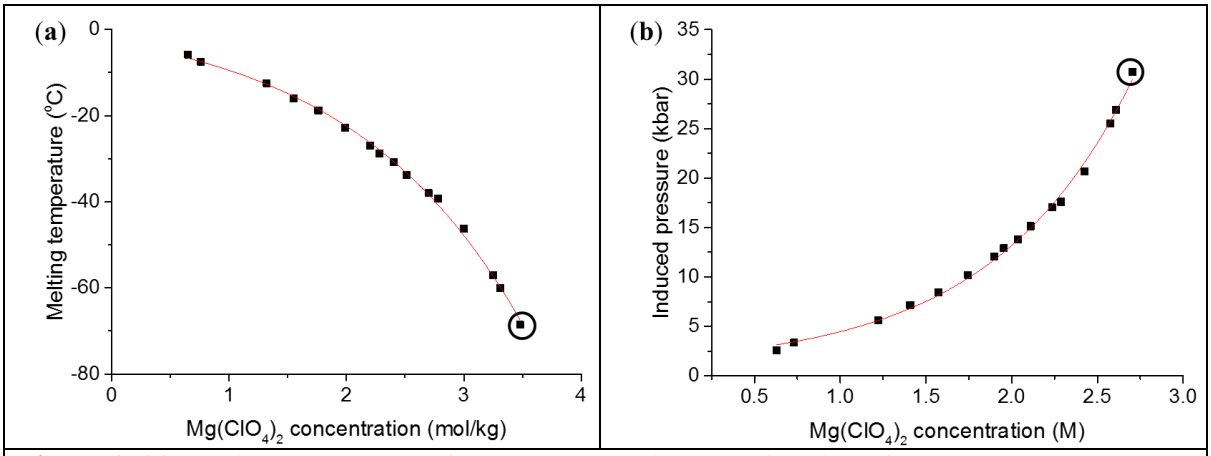

Figure 1. (a) Melting temperature of $Mg(ClO_4)_2$ solutions as a function of concentration in molality from Pestova et al(52). The circled point highlights the melting temperature at a $Mg(ClO_4)_2$ concentration of 3.48 mol/kg (44 wt%) **(b)** Pressure in kbar induced by $Mg(ClO_4)_2$ as a function of concentration in molarity M based on melting temperature data (points). This is fit using the equation $P = 1.07565 \times \exp\left(\frac{M}{0.81949}\right) + 0.82427$ where the constants were determined by fitting the data in (b) (line). The circled point highlights the induced pressure at a $Mg(ClO_4)_2$ concentration of 2.7 M (44 wt%). The circled points in (a) and (b) correspond to a $Mg(ClO_4)_2$ concentration which has been studied previously using neutron diffraction(30).

We must now attempt to estimate the pressure resisting ability of TMAO as a function of concentration, as there is no direct experimental evidence of this, such that we can choose a concentration of TMAO that will resist a pressure of 2-3 kbar. The concentration of TMAO in the muscle tissue of snailfish as a function of depth as measured by Yancey et al.(44) and shown in figure 2 shows a linear dependence. It is well known that the pressure in the ocean increases by 1 atm for every 10 metres of depth. The presence of TMAO has been suggested to be a mechanism by which the snailfish protect themselves against this increased pressure, although the exact molecular mechanism is yet to be determined. One can therefore infer the pressure resisting ability of TMAO as a function of concentration from this data, as shown in figure 2. If one extrapolates the concentration dependence on depth, and therefore equivalent pressure, one finds that 1.0 M TMAO must resist a pressure of 2.4 kbar (point circled in Figure 2(b)). The available published data and its analysis (Figures 1 and 2) therefore suggest that a 0.2 M $Mg(ClO_4)_2$ and 1.0 M TMAO mixture may provide a balance between the action of the terrestrial kosmotrope TMAO and the martian chaotrope $Mg(ClO_4)_2$.

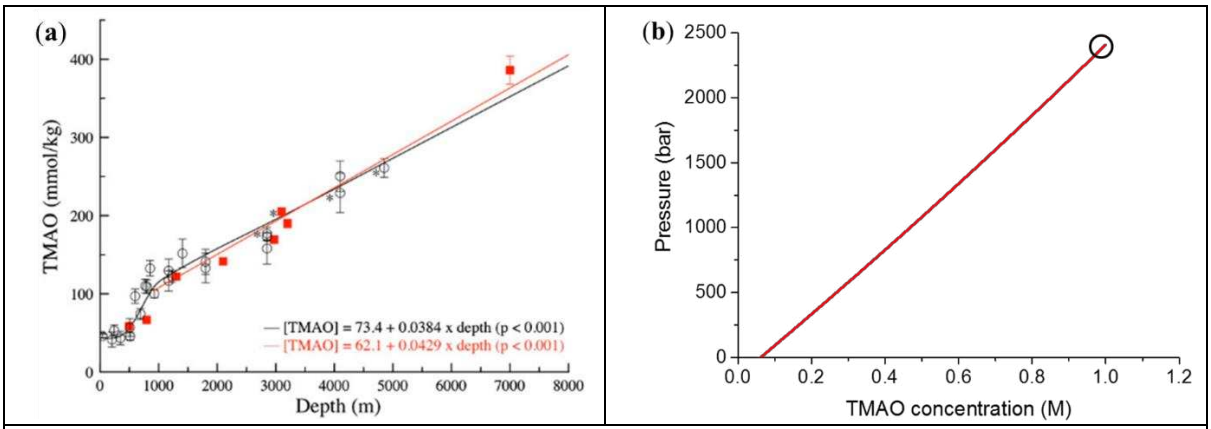

Figure 2. (a) Concentration of TMAO in mmol/kg of wet muscle tissue as a function of depth from Yancey et al(44). **(b)** Equivalent pressure P as a function of TMAO concentration M as derived from the relationship shown in red by Yancey et al. (right). The red relationship was chosen as this better fits the high concentration data. For the conversion from molality to molarity it was assumed that the density of TMAO solution changes negligibly with TMAO concentration. This is

supported by the experimental solution densities reported in table 1. Pressure relationship derived in supplementary information. $P = \left[\frac{M\times10^6}{1000-75.11M} - 62.1\right]\left[\frac{0.101325}{0.0429}\right] + 1.01325$

The question of whether TMAO can act to preserve the hydrogen bond network of water against the pressurising effect of $Mg(ClO_4)_2$will be addressed here using neutron diffraction and data analysed using empirical potential structure refinement (EPSR) to produce site-specific radial distribution functions and coordination numbers. The resulting simulated box of atoms produced by EPSR will then be analysed further using a custom built code to determine hydrogen bond angle distributions and hydrogen bond energy distributions. This allows us to study the effects of TMAO and $Mg(ClO_4)_2$ on the structure of water at a level of detail previously inaccessible to EPSR.

3. Materials and Methods

3.1. Neutron Diffraction

Neutron diffraction data were taken using the Near to InterMediate Range Order Diffractometer(54) at the ISIS Pulsed Neutron and Muon Source covering a Q range of 0.01 – 30 $Å^{-1}$. Multiple scattering, attenuation and inelastic scattering effects corrected using Gudrun software(55). This also was used to verify the amount of hydrogen present in each sample, as this has a large effect on the predicted differential scattering cross section level determined by Gudrun. This is therefore an extremely sensitive method by which to estimate any water that may have been absorbed onto the anhydrous and highly hydroscopic $Mg(ClO_4)_2$ during sample preparation. The resulting total interference differential scattering cross section $F(Q)$ can be deconstructed into its constituent partial structure factors $S_{\alpha\beta}(Q)$ between any two atomic species α and β by equation 1, where c is the concentration of a particular atomic species and b is the nuclear scattering length of a particular atomic species(56).

$$F(Q) = \sum_{\alpha\beta} c_\alpha c_\beta b_\alpha b_\beta (S_{\alpha\beta}(Q) - 1) \quad (1)$$

Performing a Fourier transform on a partial structure factor results in the radial distribution function (RDF), and integrating the RDF between a distance r_1 and r_2 yields the average number of β atoms that can be found in a spherical shell with inner radius r_1 and outer radius r_2 from an α atom located at its centre. This is more commonly known as the coordination number when the distances r_1 and r_2 correspond to the beginning and end of hydration/coordination shells around central atoms.

3.2. Sample Preparation

As neutron scattering is highly sensitive to isotope substitution, particularly hydrogen-deuterium, isotopic variants of each sample were prepared. This is assumed to have a negligible effect on structure while having a large effect on the total interference differential scattering cross section. In order to keep molar ratios constant between isotopic variants samples were prepared by weight, taking into account the different molar masses of the isotopic variants. The water in each sample was prepared using either pure H_2O, pure D_2O, or an equal mixture of the two, HDO. The TMAO used in the relevant samples was also either fully hydrogenated TMAO, fully deuterated TMAO, or an equal molar ratio of the two. This therefore yielded 3 isotopic variants for each sample not containing any TMAO, and 7 isotopic variants for each sample containing TMAO. A full table of the samples studied in this work is available in the supplementary information.

3.3. Densities of Solution

The densities of all the solutions used in this work were measured at 25°C using an Anton Parr DMA 4100 M densitometer, which gives a value in g/cm^3. The densities in terms of atoms/Å^3 were then calculated using the molar ratios and molar masses for each constituent element in each sample.

3.4. ESPR Simulations

EPSR is a Monte Carlo based simulation method that parameterises every atom in the system with a reference potential containing the Lennard Jones σ and ε parameters and a charge(3,57,58). The system is allowed to equilibrate using this reference potential, typically over several hundred Monte Carlo iterations, to produce simulated total interference scattering cross sections and provide preliminary fits to the experimental scattering data. An empirical potential is then included which further refines the simulation against the experimental scattering data over hundreds to thousands more Monte Carlo iterations to improve the quality of the simulated total interference scattering cross sections. The final result is a simulated box of atoms whose total interference scattering cross sections are consistent with the experimental neutron scattering data. This simulated box is then used to calculate radial distribution functions, coordination numbers, spatial density functions, etc.

Within EPSR a cubic box was built with the appropriate concentrations, temperatures, and densities. Details of the box dimensions and number of molecules used for each sample can be found in the supplementary information. All bond lengths, angles, Lennard Jones and Coulomb parameters were taken from previous literature on neutron scattering and EPSR analysis on aqueous TMAO(45,46) and aqueous $Mg(ClO_4)_2$(30,42). A number of force field parameters are available for TMAO(59,60). For consistency we chose the force field parameters employed in the neutron scattering and EPSR study of TMAO from Meersman et al(45,46). The final parameters and resultant fits from the EPSR simulations to the experimental total interference scattering cross sections can also be found in the supplementary information. It is important to note that EPSR yields total interference scattering cross sections that are consistent with the experimental data and based on sensible initial parameters. It does not guarantee a unique solution that perfectly matches the samples. It also fails to perfectly fit the data at low Q values as a result of insufficient correction to data or imperfectly estimated inelasticity effects. Both of these are increasingly difficult to account for at low Q, and particularly with samples containing a large proportion of light atoms. However despite these inaccuracies, it is unlikely that the overall structure resulting from EPSR is significantly effected(45).

3.5. Hydrogen Bonding Analysis Routine

In order to further analyse the results from EPSR, a custom hydrogen bonding analysis routine was written. This code first reads in the coordinates for the centre of mass of each molecule relative to the centre of the box, and the coordinates of each atom relative to its molecule's centre of mass.

It then identifies which water molecules are within the first coordination shell of each water molecule or TMAO oxygen in the box. For each of these molecules in the coordination shell it then identifies which ones are donating hydrogen bonds to the central molecule. Here we define a water molecule as donating a hydrogen bond to the central molecule if it simultaneously satisfies two conditions: The water molecule's oxygen must be within a distance to the central molecule oxygen corresponding to the first minima in the O_wO_w RDF, and its hydrogen must be within a distance to the central molecule oxygen corresponding to the first minima in the O_wH_w RDF. Water molecules donating hydrogen bonds to TMAO are defined in a similar way but treating the TMAO oxygen as the central oxygen. This topographical definition of hydrogen bonding in water has the advantage of flexibility over a variety of other criteria. Strict geometric criteria usually consider the simultaneous satisfaction of a distance constraint and an angular constraint concerning the orientation of the OH vector(61–67), and energetic criteria usually define a hydrogen bond as two molecules having an

interaction energy below a certain threshold(62,64,67,68). There also exists a definition based on the occupancy of the σ^* electron orbital on the acceptor oxygen, but this is also derived from geometric criteria(62). The definition used here allows the RDFs of the system to define the hydrogen bonding, allowing it to be applied to systems where the hydrogen bonding network of water is significantly perturbed, and to other molecular species that can accept hydrogen bonds. Under these circumstances any geometric or energetic cut offs would be inapplicable by definition.

Based on this definition of hydrogen bonding the code is then able to evaluate the hydrogen bond donor angle and the total interaction energy between every atom in the hydrogen bonded molecule pair. The donor angle is defined as the angle between the vector pointing from the donor oxygen to the acceptor oxygen and the vector pointing from the donor oxygen to the donor hydrogen, and the total interaction energy is defined as the sum of the electric potential energy and the Lennard-Jones interaction energy between every atom in hydrogen bonded molecule pair. This allows for a distribution of bond angles and bond energies to be obtained. The average number of water molecules hydrogen bonded to a central water or TMAO molecule is also obtained, as well as the number of water molecules in the system that are hydrogen bonded to other water molecules in cyclic dimer or bifurcated oxygen conformations. These are conformations water molecules undergo during hydrogen bond switching events, and so counting them gives a measure of the instability of the hydrogen bond network.

After the EPSR simulation had been run for a large number (>1000) of iterations to ensure the system was well equilibrated and had explored a large conformational space, the relevant distributions, hydrogen bond counts and conformations were obtained. EPSR was then iterated once and the process repeated. This was repeated 20 times to improve the statistical significance of the results.

4. Results

4.1. Density of solutions

The bulk densities of all six samples measured at 25°C and using fully hydrogenated isotope constituents are given in table 1 below.

Sample	**Density** (g/cm^3) ± 0.0001
Pure H_2O	0.9970
1.0 M TMAO	0.9994
2.7 M $Mg(ClO_4)_2$	1.3770
1.0 M TMAO, 2.7 M $Mg(ClO_4)_2$	1.3513
0.2 M $Mg(ClO_4)_2$	1.0281
1.0 M TMAO, 0.2 M $Mg(ClO_4)_2$	1.0275
Table 1. Densities of solutions as measured at 25°C using a densitometer	

As shown in table 1, the introduction of 1.0 M TMAO causes a slight increase in density, likely simply due to the introduction of a larger molecule into the system. 2.7 M $Mg(ClO_4)_2$ shows a large increase in the density of the solution, but the introduction of 1.0 M TMAO into 2.7 M $Mg(ClO_4)_2$ causes a reduction in density again, consistent with our hypothesis that TMAO is acting to overcome the pressurising effect of the $Mg(ClO_4)_2$. The same effect is observed to a lesser extent at the lower concentration of 0.2 M $Mg(ClO_4)_2$.

4.2. Radial Distribution Functions

In order to assess whether TMAO can restore the hydrogen bond network of water against the perturbation caused by $Mg(ClO_4)_2$ neutron scattering experiments were completed on pure water to provide a reference. This was to ensure that all samples were prepared in an identical manner and data was treated in the same way with regards to inelasticity corrections and EPSR analysis to allow for the

most reliable possible comparison. EPSR was performed on the resulting corrected scattering data and a high quality fit was achieved as shown in figure 3. The resulting fits for the other 4 samples were to a similar standard as shown in the supplementary material.

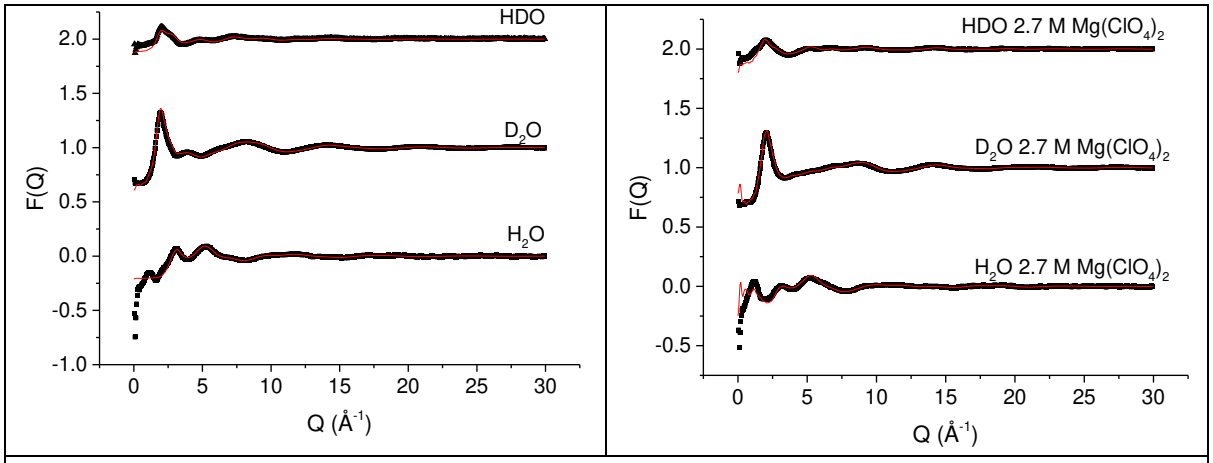

Figure 3. EPSR fits (red lines) to corrected diffraction data (black points) for the three isotopic variants on pure water (left) and the three isotopic variants of 2.7 M $Mg(ClO_4)_2$ (right)

As with previous results, the tetrahedral nature of pure water was observed by studying the O_wO_w RDF as derived from the resultant EPSR simulation. A first strong peak was detected at 2.78 Å and a second weaker peak was detected at 4.45 Å, consistent with a tetrahedral arrangement of the water molecules. The O_wO_w RDFs for all 6 samples investigated in this research can be seen in figure 4.

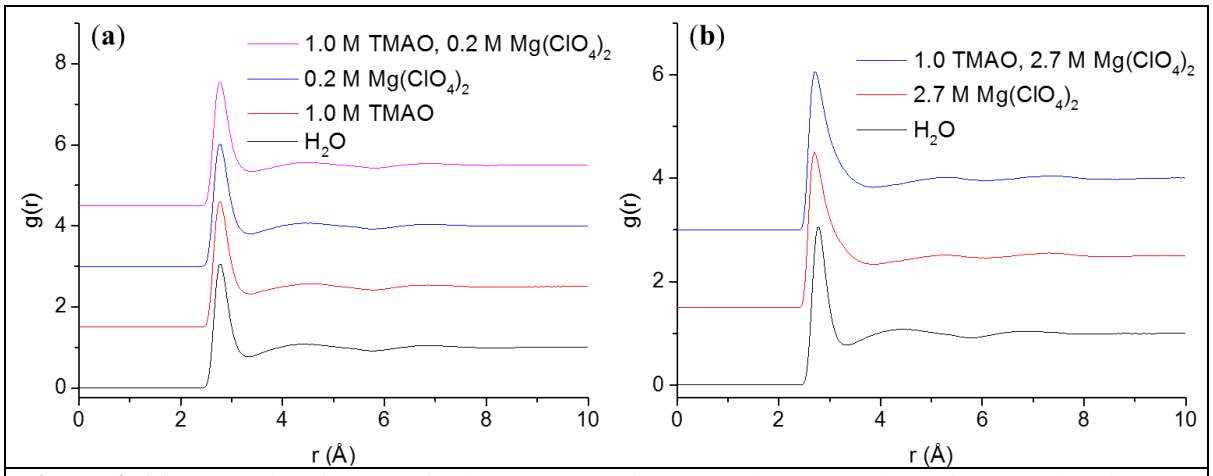

Figure 4. (a) O_wO_w site-site RDF for low concentration $Mg(ClO_4)_2$ samples. **(b)** O_wO_w site-site RDF for high concentration $Mg(ClO_4)_2$ samples. RDFs vertically offset for clarity.

The positions of the first and second peaks for all samples are illustrated in table 2. The positions of the peaks were determined by fitting a Gaussian function to the very top of the peak, and the uncertainties in peak location are therefore the uncertainties associated with the Guassian fitting. As the large number of iterations within EPSR generate extremely smooth RDFs the top of the peaks can all be fit very closely to a Guassian and the uncertainties were therefore smaller than the quoted precision. It is important to note that the second peak for both samples containing 2.7 M $Mg(ClO_4)_2$ actually corresponds to an inward movement of the third peak of the pure water sample. The second peak in the pure water sample is a result of the second hydration shell, but in the presence of 2.7 M $Mg(ClO_4)_2$ this has completely collapsed into the first hydration shell, as shown in figure 5(b). These results are consistent with the results from the first study done on aqueous $Mg(ClO_4)_2$(30).

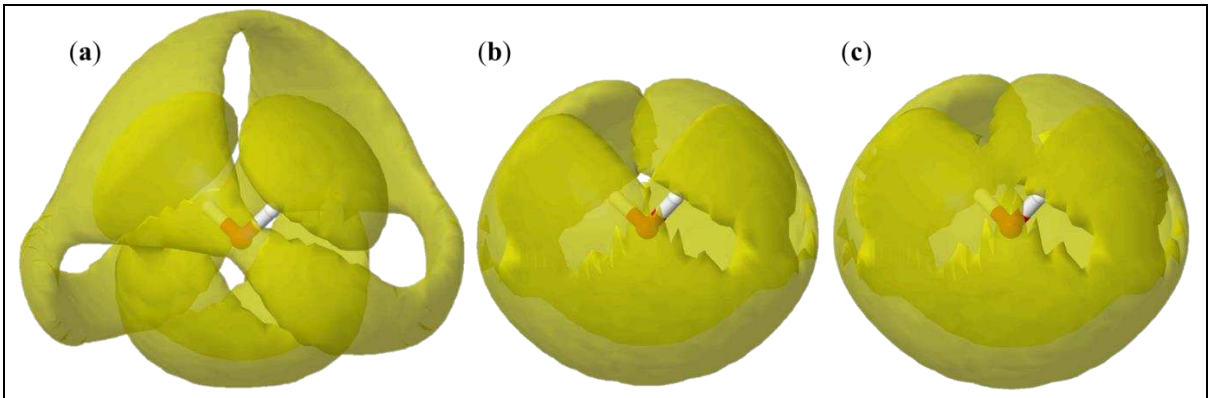

Figure 5. Spatial density functions of water around a central water molecule from neutron diffraction data and EPSR analysis for pure water (**a**), 2.7 M $Mg(ClO_4)_2$ (**b**), and 1.0 M TMAO + 2.7 M $Mg(ClO_4)_2$ (**c**). These surface contours contain the highest 30% probability areas of finding another molecule within a distance of 5 Å from the central molecule

In agreement with previous studies,(30) the impact of $Mg(ClO_4)_2$ on the structure of water is more pronounced in the second hydration shell than the first due to steric hindrance. The addition of 1.0 M TMAO to pure water results in a more expanded structure relative to pure water with the second hydration shell moving outwards by 0.11 Å as shown in figure 4(a). Again, in agreement with previous studies(30) the presence of 2.7 M $Mg(ClO_4)_2$ causes the second peak to be completely pushed into the first peak, and the third peak to be drawn inwards from 6.89 Å to 5.27 Å, as shown in figure 4(b). The pressurising effect is so significant that the first peak also experiences an inward movement, with the position of the first hydration shell reducing from 2.78 Å to 2.71 Å. The addition of 1.0 M TMAO to 2.7 M $Mg(ClO_4)_2$ results in both the first and the second peak to shift back outwards only very slightly, as shown in figure 4(b) and figure 5(c).

Sample	**First Peak Location** (Å)	**Second Peak Location** (Å)
Pure H_2O	2.78	4.45
1.0 M TMAO	2.77	4.56
2.7 M $Mg(ClO_4)_2$	2.71	5.27
1.0 M TMAO, 2.7 M $Mg(ClO_4)_2$	2.72	5.29
0.2 M $Mg(ClO_4)_2$	2.78	4.49
1.0 M TMAO, 0.2 M $Mg(ClO_4)_2$	2.77	4.50

Table 2. Peak locations for O_wO_w RDFs for all samples. Uncertainties not quoted as very high quality Gaussian fits to the tops of the RDF peaks yielded an associated uncertainty smaller than the quoted precision.

This effect is also observed in the 1.0 M TMAO + 0.2 M $Mg(ClO_4)_2$ sample. Contrary to expectations, 0.2 M $Mg(ClO_4)_2$ results in a slight outward shift of the second coordination shell relative to pure water rather than an inward one, however the relationship observed between the second peak location of 0.2 M $Mg(ClO_4)_2$, 1.0 M TMAO, and the combined 1.0 M TMAO + 0.2 M $Mg(ClO_4)_2$ sample still supports the hypothesis that TMAO is acting to resist the perturbations to water structure induced by $Mg(ClO_4)_2$. This hypothesis is further supported when considering the height of the first peak. The addition of 1.0 TMAO causes a slight increase in peak height. The addition of 2.7 or 0.2 M $Mg(ClO_4)_2$ causes a roughly equal reduction in peak height relative to pure water, whereas the combined samples at both $Mg(ClO_4)_2$ concentrations result in a relatively unchanged peak height.

4.3. Coordination numbers

The average coordination number for particular molecules around a central molecule in each sample is calculated by integrating the relevant RDF over a distance corresponding to its first minima (see

supporting information for full description of coordination number and calculation distances). The value for pure water, calculated over a distance of 3.33 Å corresponding to the first minima in the O_wO_w RDF, was given as 4.41 ± 0.02 molecules. Here the uncertainties are calculated by fitting a Gaussian peak to the histogram of coordination numbers produced by EPSR as a result of >1000 iterations, and do not include the effects of (unknown) systematic uncertainties in the original scattering data and in the EPSR method. An example of this is provided in the supplementary information. This is slightly lower than the value of 4.67 ± 0.01 given in the literature(3), however this latter value was calculated over 3.36 Å. The addition of 2.7 M $Mg(ClO_4)_2$ increases the average coordination number to 5.752 ± 0.009 calculated over 3.73 Å. Contrary to the hypothesis that TMAO can resist the pressurising effect of $Mg(ClO_4)_2$ on water structure, which would be reflected in an average coordination number decrease, the coordination number is shown to increase upon the subsequent addition of 1.0 M TMAO to 5.89 ± 0.01. However this is calculated over a larger distance of 3.83 Å. It is difficult to comment on whether these findings support the hypothesis or not as they are calculated over different distances in each case and each sample has a different excluded volume effect as a result of the solute addition which will directly affect the resulting coordination number. What is clear however when considering the results from the RDFs, the overall similarity of the RDFs, and the coordination numbers is that the conventional quantitative methods employed by EPSR are not capable of revealing very subtle changes in the network. In order to investigate the hypothesis further a more detailed analysis tool is required.

4.4. Hydrogen Bonding Conformation and Energy Analysis

4.4.1. *Water-water hydrogen bonding*

The average number of water molecules donating a hydrogen bond to a central water molecule was measured, which was then doubled to get the total number of hydrogen bonds per water molecule as there must be exactly as many acceptors as donors in pure liquid. The uncertainties are calculated using the standard deviation of the values for the average number of hydrogen bonds per molecule from the 20 iterations as described in the methods section. For pure water the average number of water molecules hydrogen bonded to a central water molecule was determined to be 3.412 ± 0.004, consistent with previous results(5,8,62,64,68). In 1.0 M TMAO this number decreases to 3.232 ± 0.005, likely due to an excluded volume effect. While these uncertainties are extremely small, because all samples have been treated the same way by both Gudrun and EPSR, we can still use the *trends* in the hydrogen bond numbers to draw conclusions about the nature of the hydrogen bonding in each solvent environment, even though the absolute accuracy may be poorer than quoted here. The highly perturbed hydrogen bond network induced by 2.7 M $Mg(ClO_4)_2$ is reflected by a significant decrease in the average number of hydrogen bonds per molecule to 2.005 ± 0.002. However the subsequent addition of 1.0 M TMAO results in a slight increase to 2.052 ± 0.002. Although small, this increase in the average number of hydrogen bonds per water molecule upon addition of TMAO is particularly striking in light of the fact that TMAO will have the effect of reducing the volume available for water molecules to donate hydrogen bonds to a central molecule. However, this excluded volume effect appears to be more than compensated for by the way TMAO restructures the system. A similar increase in hydrogen bond number is also observed when 1.0 M TMAO is added to 0.2 M $Mg(ClO_4)_2$ (see table in supporting information). This is in complete agreement with our hypothesis that TMAO is able to resist the perturbation to water structure induced by $Mg(ClO_4)_2$.

The hydrogen bond donor angle distribution and the total interaction energy distribution between two hydrogen bonded molecules for all six samples were calculated as described previously (see supporting information for distributions). It is important to note that the bond angle distributions peak at a positive value because the calculation of the angle between the vectors as described in section 3.5 effectively reduces a 3D problem to a 2D problem. In reality this angle represents the angle formed by the cone described by the orientation of the OH bond towards the acceptor oxygen (see supporting information for diagram). Averaging this value over the solid angle therefore means a most probable

angle in 3D of 0 degrees. The hydrogen bond angle distributions were fit using equation 2 below to determine the peak location x_c where x is the binned donor angle, y is the frequency of occurrence, A is the amplitude, and w is the width. This fits the general distribution shapes shown in figure 6(a) well around the peak and is therefore a useful mathematical tool for determining peak location. However it is nonzero at $x = 0$ and therefore cannot contain any physical relevance as at 0^o the solid angle becomes 0 and therefore any probability distribution function must also be 0. The final calculated parameters from this function for each of the 6 samples are presented in the supporting information. The bond energy distributions were fit using a Gaussian distribution.

$$y = \mathrm{y}_0 + A\exp(-\exp(-z) - z + 1) \qquad (2)$$
$$z = \frac{x - x_c}{w}$$

While these results reveal more detail than simply observing the RDFs, the changes are still very subtle and not easily visible by direct comparison of the distributions, as shown in figure 6. The response of the hydrogen bonding characteristics of the bulk water are more easily visualised using a conformational energy density map, where the donor angle and energy of each hydrogen bond are plotted simultaneously. These results, along with the fitting results of the bond angle and energy distributions are shown in figure 7 below. Each point is coloured according to the normalized density of points around it and colours are separated at the boundaries described in figure 7. An exact description of the mathematics behind these plots is well described in the OriginLab user guide(69), and will not be discussed here. This is kept consistent for all samples to allow for direct comparison. It is important to note that the water density map has significantly fewer points. This is because the pure water simulations used a smaller box of molecules as this allows for a faster simulation and there was no need to account for solute molecules. There are also significantly fewer points in the samples containing 2.7 M $Mg(ClO_4)_2$ as the highly distorted pressurised network meant there are fewer hydrogen bonds detected.

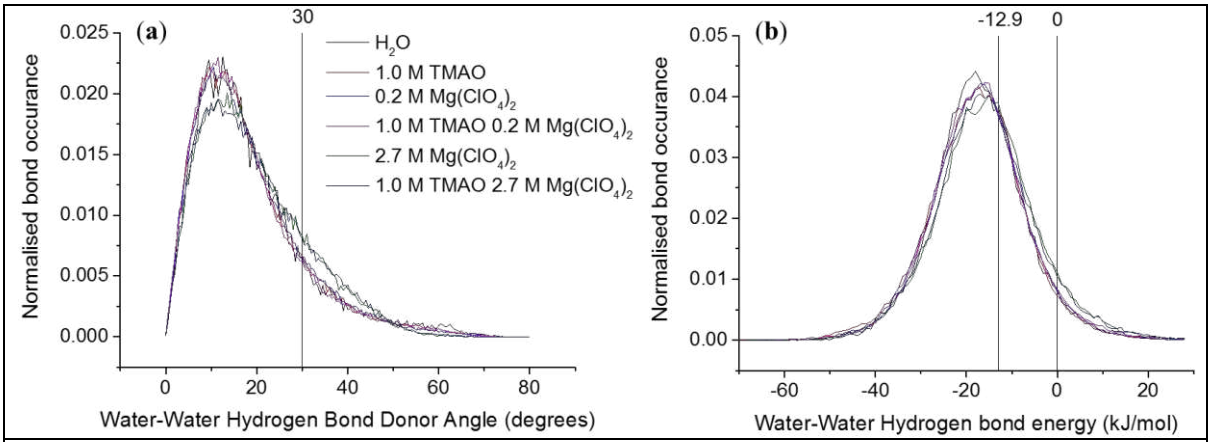

Figure 6. (a) Water-water hydrogen bond angle distribution.(**b**) hydrogen bond energy distribution. A vertical line at 30 degrees is included in the bond angle distributions and a vertical line at -12.9 kJ/mol is included in the energy distributions as these represent typically employed energetic and geometric cut-offs for hydrogen bonding(18,62,64,65,68).

Here we see that pure water (fig. 7(a)) has a well-defined sharp peak, indicated by the grey area in the conformational energy density map. This can be thought of as a reflection of the most intact and most stable hydrogen bond network, with the lowest average hydrogen bond interaction energy, and highest number of hydrogen bonds per water molecule. The addition of 1.0 M TMAO into pure water (fig. 7(b)) results in a slight decrease in the angle peak location and a straighter average water-water hydrogen bond, consistent with the more expanded network of water indicated by the movement of the second peak of the O_wO_w RDF outwards. This is accompanied by a reduction in stability of the average

water-water hydrogen bond indicated by an increase in the average bond energy. Such a change is likely due to strong interactions between the water molecules hydrating the TMAO molecule and leading to a decrease of stability in the bulk. These changes to the network are reflected in the conformational energy density map as the very high density grey area present in pure water disappears in the presence of 1.0 M TMAO as the peak becomes less sharp. This translates to a less well defined network and is likely due to an excluded volume effect of the TMAO. Hydration of the molecule causes a local distortion of the network in order to accommodate the solute. All these effects are also observed using the same justifications for 0.2 M $Mg(ClO_4)_2$ (fig. 7(e)).

The presence of 2.7 M $Mg(ClO_4)_2$ (fig. 7(c)) results in a much more distorted network, indicated by the angle distribution peak location increase, and a large increase in the average bond energy. This is consistent with the pressure-like effect, as hydrogen bonds must get more distorted and weaker in order to accommodate more neighbours in the first hydration shell. This large distortion is reflected in the conformational energy density map as the high density red area completely disappears, again meaning a less well defined peak and therefore a more poorly defined and distorted hydrogen bonding network. The introduction of 1.0 M TMAO to this system (fig. 7(d)) then results in a slight straightening of the bonds again, albeit within the uncertainty of the bond angle peak location, and a reduction of the average hydrogen bond energy back towards the value for pure water. The high density red area also slightly recovers, meaning a more well defined peak relative to 2.7 M $Mg(ClO_4)_2$, as the network distortion is reduced. This is consistent with the hypothesis that TMAO is helping to restore the hydrogen bond network against the perturbations induced by $Mg(ClO_4)_2$. These effects are also observed for the introduction of 1.0 M TMAO to 0.2 M $Mg(ClO_4)_2$ (fig. 7(f)), however in this case the high density red area expands to fill a greater range of angles and energies. This suggests a plateau rather than a peak in the conformational energy density map, but with an increased gradient around the plateau. This is likely a result of a larger excluded volume effect than either of the solutes individually and reflects a distorted, but overall more stable, network as shown by the values for the average interaction energy between two hydrogen bonded molecules.

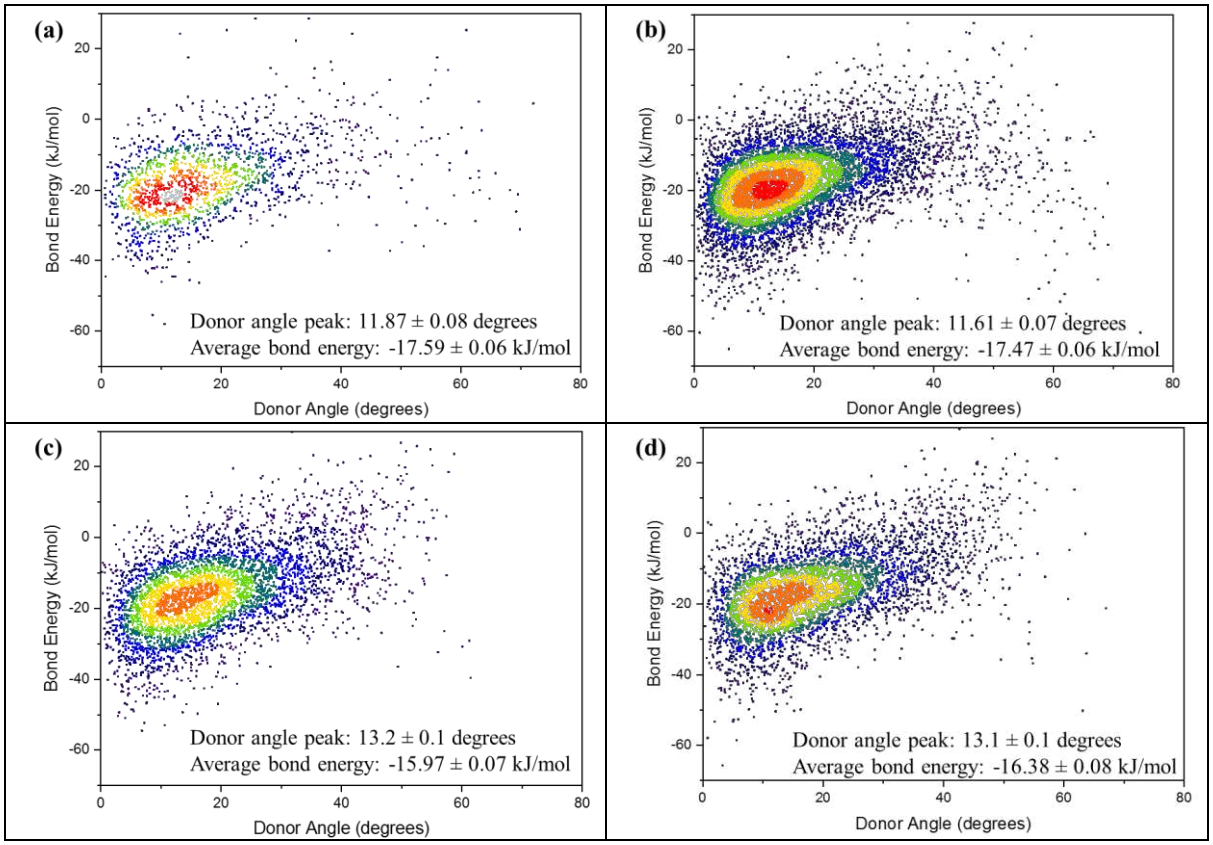

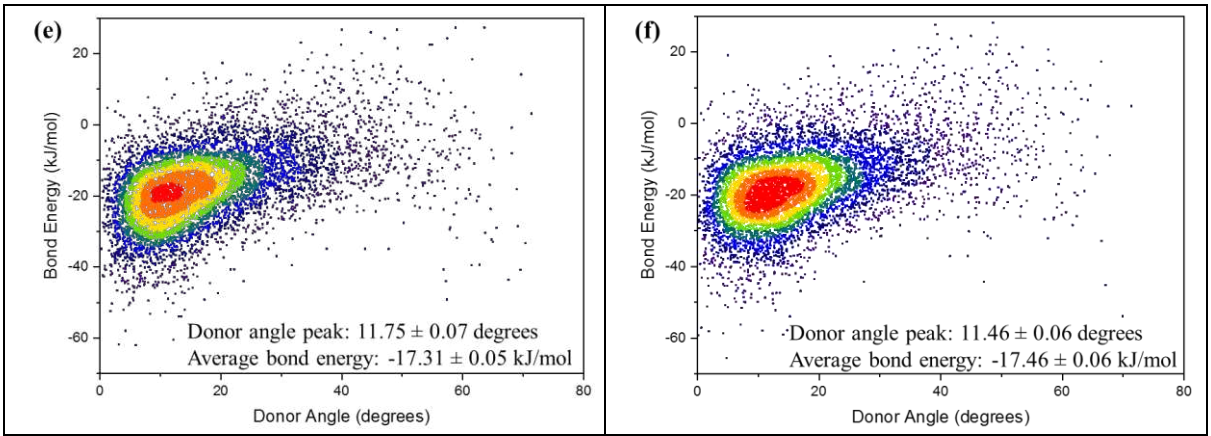

Figure 7. Conformational energy density maps for water-water hydrogen bonding for all samples. **(a)** Pure H_2O, **(b)** 1.0 M TMAO, **(c)** 2.7 M $Mg(ClO_4)_2$, **(d)** 2.7 M $Mg(ClO_4)_2$ + 1.0 M TMAO, **(e)** 0.2 M $Mg(ClO_4)_2$, **(f)** 0.2 M $Mg(ClO_4)_2$ + 1.0 M TMAO. Level boundaries correspond to: grey > 0.00196, red = 0.00171, orange = 0.00147, yellow = 0.00123, green = 0.00098, dark green = 0.000735, blue = 0.00049, dark blue = 0.000245, purple < 0.000245.

4.4.2. TMAO-water hydrogen bonding

The average number of water molecules donating a hydrogen bond to the TMAO oxygen and associated uncertainties are calculated using the same method as previously. In 1.0 M TMAO 2.191 ± 0.008 water molecules form hydrogen bonds with the TMAO oxygen, consistent with previous results(45). Upon the addition of 0.2 M $Mg(ClO_4)_2$ this is reduced to 2.014 ± 0.007, and increasing the concentration further to 2.7 M results in a further reduction to 1.33 ± 0.01. It is clear that as the concentration of $Mg(ClO_4)_2$ increases, the ability of TMAO to form hydrogen bonds with the surrounding water molecules is reduced. This is likely due to direct interaction between the positively charged Mg^{2+} ion and the negatively charged TMAO oxygen. This both limits the volume available for water molecules to occupy and donate a hydrogen bond to the TMAO oxygen, and electrostatically screens the negative charge on the TMAO oxygen inhibiting its ability to act as a hydrogen bond acceptor. These effects are illustrated by the bond angle and bond energy distributions (see supporting information). Determining the peak locations as previously shows that as the concentration of $Mg(ClO_4)_2$ increases the peak value for the bond angle first decreases then increases, and the average bond energy increases. In 1.0 M TMAO the hydrogen bond donor bond angle is 9.9 ± 0.2° and the bond energy is -35.5 ± 0.3 kJ/mol. These values then become 9.3 ± 0.1° and -31.8 ± 0.2 kJ/mol respectively in the presence of 0.2 M $Mg(ClO_4)_2$, and 11.2 ± 0.1° and -30.4 ± 0.4 kJ/mol respectively in the presence of 2.7 M $Mg(ClO_4)_2$. These results are consistent with direct interaction between the Mg^{2+} ion and the TMAO oxygen causing a reduction in the stability of TMAO-water hydrogen bonds. In all cases however the hydrogen bond between a water molecule and a TMAO molecule is much stronger than the hydrogen bond between two water molecules, as has been previously reported(45,47,50,70).

4.5. Unstable Hydrogen Bond Configurations

While EPSR is a Monte Carlo based technique and therefore incapable of quantifying the lifetimes of various conformations within the system, it can provide information on the fractions of energetically unfavourable or metastable conformations in the system. As a water molecule switches hydrogen bond partners, the hydrogen bond switching between molecules typically goes through an intermediate state where two water molecules are hydrogen bonded together through two bent hydrogen bonds. These intermediate states can be either bifurcated oxygens (BOs) or cyclic dimers (CDs)(71). The conformational landscape of the system can then be assessed in three ways: calculating the fraction of

molecules in CD conformations, calculating the fraction of molecules in BO conformations, and calculating the fraction of molecules that have positive hydrogen bond interaction energies. These conformations are energetically unfavourable and are likely to be short lived and in the process of switching their hydrogen bonding partner. The percentage of molecules in these conformations as a function of $Mg(ClO_4)_2$ concentration both with and without 1.0 M TMAO can be seen in figure 8 below.

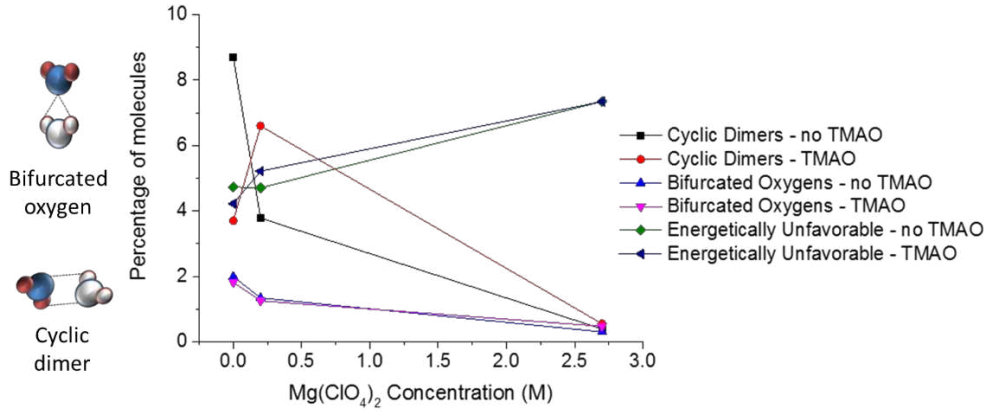

Figure 8. Percentage of molecules in cyclic dimer, bifurcated oxygen, or energetically unfavourable conformations

Here we can see that in the absence of TMAO the fraction of both cyclic dimers and bifurcated oxygens decrease with increasing $Mg(ClO_4)_2$ concentration. The fraction of energetically unstable molecules initially decreases slightly, before increasing with increasing $Mg(ClO_4)_2$ concentration . In the presence of TMAO the fraction of bifurcated oxygens decreases with increasing $Mg(ClO_4)_2$ concentration, but the fraction of cyclic dimers has an sharp initial increase before decreasing at the high $Mg(ClO_4)_2$ concentration. The fraction of energetically unfavourable molecules also increases with increasing $Mg(ClO_4)_2$ concentration.

5. Discussion

5.1. Structural Analysis

As seen previously, the effect of $Mg(ClO_4)_2$ is to perturb the structure of water in a manner similar to that of a large external pressure(30) and strongly reduce, but not eliminate, hydrogen bonding in the system(42). The results described in sections 4.1 – 4.4 suggest that TMAO is partially capable of resisting the perturbation to water structure induced by $Mg(ClO_4)_2$. Conventional analysis methods show that at concentrations of both 0.2 M and 2.7 M $Mg(ClO_4)_2$, the addition of 1.0 M TMAO causes the density of solution to reduce, the position of the second peak in the O_wO_w RDF to shift outwards, and the height of the first peak in the O_wO_w RDF to return to the value observed for pure water. More in depth analysis of the hydrogen bonding in the system reveals that the addition of 1.0 M TMAO to both concentrations of $Mg(ClO_4)_2$ results in an increase of the average number of water molecules hydrogen bonded to a central molecule, a decrease in the peak value for the water-water hydrogen bond donor angle, and a decrease in the average hydrogen bond energy between water molecules. All of these results suggest that the addition of TMAO to $Mg(ClO_4)_2$ solution results in a more expanded and more stable hydrogen bonding structure, more reminiscent of pure water. Examining these results in detail however does show that the resisting effects are only slight. Hence the stabilising effect of TMAO on proteins against chaotropic ions like those used in this study likely comes from an additional effect and is not solely due to water structure modification. It is worth noting that while we have focused on the hydrogen bond angles and energy conformations, the distribution of hydrogen bonding conformations may be a compensation between the entropy and energy of hydrogen bonds. Other studies in the literature have included this analysis(72,73), however without a series of neutron

scattering experiments on the system presented here at different temperatures it is not possible to deconvolute these effects.

While we have presented the first study of water structure in TMAO-$Mg(ClO_4)_2$ solutions, it is interesting to consider how these results compare with the more well studied system of TMAO-urea. A previous neutron diffraction study of TMAO-urea solutions showed that the oxygen atom on TMAO preferentially forms hydrogen bonds with urea(45). In the context of a protein in a urea-water solution, urea-induced denaturation is thought to act via a direct mechanism, with urea binding to the protein backbone and side chains, with little perturbation to water structure(74–77). Conversely, the mechanism by which TMAO stabilises proteins remains debated. While some studies have suggested depletion effects associated with unfavourable interactions of TMAO with the protein backbone(78–80), other studies have suggested that TMAO interacts favourably with polypeptides(81,82). The counteracting effect of TMAO on urea also remains controversial with some studies arguing that TMAO decreases the protein solubility by modifying the urea and water structure around the protein, leading to protein compaction(83,84). While others have argued that TMAO does not modify urea structure around protein(85,86). In a recent study TMAO was found to counteract the denaturing effects of urea by inhibiting protein-urea preferential interactions and the extent of counteraction is heavily dependent on the amino acid composition of the peptide(87). These studies highlight the importance of the choice and presence of protein when examining the counteracting action of TMAO and urea. While in the present study we have focused on the impact of TMAO and $Mg(ClO_4)_2$ on water structure, future studies which include a polypeptide will allow combined action of these important solutes.

5.2. Unstable Conformation Analysis

As mentioned in section 4.5, EPSR is a Monte Carlo based technique and therefore incapable of directly measuring the hydrogen bonding dynamics of the system. However, we can use the data to study the relative fractions of energetically unstable intermediates or energetically unfavourable conformations in the system.

Let us first consider the effect of adding 1.0 M TMAO to pure water. In this case the relative proportion of bifurcated oxygens, cyclic dimers, and energetically unfavourable conformations all decrease. This is consistent with previous findings that TMAO causes an enhanced hydrogen bond lifetime between water molecules(47,50,70,88), and therefore fewer conformations associated with hydrogen bond switching should be observed. This is also the case for the addition of 0.2 M $Mg(ClO_4)_2$ to pure water. All three criteria decrease, consistent with previous findings that strong interactions between water molecules and Mg^{2+} and ClO_4^- ions cause an increase in hydrogen bond reorientation time(9,17,19,20,22). The ability to calculate distributions of the interaction energies between ions and water molecules was not included in the hydrogen bonding analysis routine. However, the positions of the relevant peaks in the water-ion RDFs, as shown in the supplementary information, suggest that the average interaction energy between an Mg^{2+} ion and a neighbouring water molecule is approximately -438 kJ/mol, and the average interaction energy between a ClO_4^- ion is approximately -37 kJ/mol. The strong interactions seen in previous research are therefore also observed here(9,17,19,20,22).

Now let us consider the combined effect of 0.2 M $Mg(ClO_4)_2$ and 1.0 M TMAO. As previously the bifurcated oxygen proportion continues to decrease to a level lower than each individual case, however the cyclic dimer proportion increases from 3.70% in 1.0 M TMAO or 3.78% in 0.2 M $Mg(ClO_4)_2$ to 6.60% in the combined case. This represents a movement back towards the value for pure water, which is determined to be 8.70%. This is also the case for the fraction of energetically unfavourable conformations. In 1.0 M TMAO and 0.2 M $Mg(ClO_4)_2$ the fraction of energetically unfavourable conformations are 4.22% and 4.71% respectively. In the combined case this increases to 5.22%. This actually surpasses the value determined for pure water of 4.73%. The data therefore suggests that in

the low concentration samples the combined effect of $Mg(ClO_4)_2$ and TMAO restores the structure of water. These results are likely due to the interaction between the Mg^{2+} ion and the TMAO oxygen. The MgO1 RDF in the supplementary information shows a very sharp, but likely overestimated, peak, indicating a strong interaction between the two species. This screens the electrostatic interaction between the Mg^{2+} ion or the TMAO oxygen with the surrounding water molecules, and effectively eliminates strong hydrogen bonding sites from the system. This is also consistent with the results described in section 4.4.2, which shows increasing $Mg(ClO_4)_2$ concentration reduces the number of water molecules forming hydrogen bonds with the TMAO oxygen.

Finally let us consider the relative proportions of unstable intermediates for 2.7 M $Mg(ClO_4)_2$ both with and without TMAO. 2.7 M $Mg(ClO_4)_2$ shows a very low proportion of cyclic dimers, 0.39%, and bifurcated oxygens, 0.30%. Upon the addition of 1.0 M TMAO, both of these values then slightly increase to 0.55% and 0.47% respectively, consistent with the results from the low concentration sample and can again be explained by association of the Mg^{2+} ion and the TMAO oxygen resulting in weaker hydrogen bonding sites. When considering the fraction of energetically unfavourable conformations, the presence of 2.7 M $Mg(ClO_4)_2$ causes a large increase relative to pure water, from 4.73% to 7.35% both with and without 1.0 M TMAO. These results are seemingly somewhat contradictory, as both are measures of instability of the system, yet one increases while the other decreases. We rationalise this contradiction by suggesting that the extreme perturbation to the hydrogen bond network and reduction in hydrogen bond stability at high $Mg(ClO_4)_2$ concentration means that it is no longer significantly energetically favourable to adopt an intermediate BO or CD conformation while switching hydrogen bond partners. The reduced hydrogen bond stability means that water molecules can switch partners through energetically unfavourable conformations that are not typically observed intermediates.

6. Conclusion

Based on the results presented in this work we can conclude that TMAO is partially capable of restoring the water hydrogen bond network against the perturbations induced by $Mg(ClO_4)_2$. The structure of bulk water, as evidenced by the density, O_wO_w RDFs, and the calculated hydrogen bonding parameters, is more similar to that of pure water when TMAO is added to aqueous $Mg(ClO_4)_2$. However, as the effects are only slight, the ability of TMAO to stabilise proteins against chaotropic ions likely comes from an additional effect and is not solely due to water structure modification. The effect on the relative proportion of unstable BO or CD intermediates and energetically unfavourable conformations is likely due to the strong interaction between the Mg^{2+} ion and the TMAO oxygen electrostatically screening each other and effectively eliminating the strong hydrogen bonding sites. This causes these proportions to return towards the values recorded for pure water. This work also introduces a topographical definition of hydrogen bonding that is well suited to EPSR analysis, and yields an average number of water molecules hydrogen bonded to a central molecule and an average hydrogen bond energy between two water molecules that are consistent with previous literature(5,8,62,64,68). The resulting bond angle and bond energy distributions help to illustrate some of the inadequacies with purely energetic or geometric constraints. Many hydrogen bonds may be much less stable, and much more bent, than one would reasonably assume. This also supports our previous work which states that even in concentrated $Mg(ClO_4)_2$ solutions, hydrogen bonding between molecules in the system is not completely destroyed(42).

Acknowledgements

Experiments at the ISIS Pulsed Neutron Facility were supported by a beam time allocation from the Science and Technology Facilities Council under proposal number RB1910455. The authors thank Tristan Youngs and Thomas Headen for their support during the running of the neutron diffraction experiments and Catherine Walsh, University of Leeds for fruitful discussions on astrochemistry and

molecular astrophysics. The project was supported by a grant from the Engineering and Physical Sciences Research Council (EPSRC) (EP/P02288X/1) to L. Dougan and an ISIS Facility Development and Utilisation Studentship to H. Laurent. All data is available at https://doi.org/10.5518/759 under a Creative Commons Attribution license (CC-BY).

References

1. Marcus Y. Effect of ions on the structure of water: Structure making and breaking [Internet]. Vol. 109, Chemical Reviews. 2009 [cited 2017 Nov 1]. p. 1346–70. Available from: http://0-pubs.acs.org.wam.leeds.ac.uk/doi/pdf/10.1021/cr8003828

2. Ball P. Water is an active matrix of life for cell and molecular biology. Proc Natl Acad Sci [Internet]. 2017 [cited 2018 Nov 15];114(51):13327–35. Available from: www.pnas.org/cgi/doi/10.1073/pnas.1703781114

3. Soper a. K. The Radial Distribution Functions of Water as Derived from Radiation Total Scattering Experiments: Is There Anything We Can Say for Sure? ISRN Phys Chem [Internet]. 2013;2013:1–67. Available from: http://www.hindawi.com/journals/isrn/2013/279463/

4. Amann-Winkel K, Bellissent-Funel MC, Bove LE, Loerting T, Nilsson A, Paciaroni A, et al. X-ray and Neutron Scattering of Water. Chem Rev [Internet]. 2016 [cited 2018 Nov 19];116(13):7570–89. Available from: https://pubs.acs.org/sharingguidelines

5. Zhao L, Ma K, Yang Z. Changes of water hydrogen bond network with different externalities. Int J Mol Sci [Internet]. 2015 Apr 15 [cited 2017 Oct 10];16(4):8454–89. Available from: http://www.mdpi.com/1422-0067/16/4/8454/

6. Ma K, Zhao L. The opposite effect of metal Ions on short-/long-range water structure: A multiple characterization study. Int J Mol Sci. 2016;17(5).

7. Dillon SR, Dougherty RC. Raman studies of the solution structure of univalent electrolytes in water. J Phys Chem A [Internet]. 2002 [cited 2017 Oct 18];106(34):7647–50. Available from: http://0-pubs.acs.org.wam.leeds.ac.uk/doi/pdf/10.1021/jp020655h

8. Nucci N V, Vanderkooi JM. Effects of salts of the Hofmeister series on the hydrogen bond network of water. J Mol Liq [Internet]. 2008 [cited 2018 Nov 13];143(2–3):160–70. Available from: https://ac.els-cdn.com/S0167732208001694/1-s2.0-S0167732208001694-main.pdf?_tid=e55ed1a7-9d99-4f19-a053-410d57eebf66&acdnat=1542122798_e66d99bc381a4668227785fd96453c56

9. Zhang Q, Pan Z, Zhang L, Zhang R, Chen Z, Jin T, et al. Ion effect on the dynamics of water hydrogen bonding network: A theoretical and computational spectroscopy point of view [Internet]. Vol. 8, Wiley Interdisciplinary Reviews: Computational Molecular Science. 2018 [cited 2019 Sep 9]. p. 1373–96. Available from: https://doi.org/10.1002/wcms.1373

10. Max J-J, Chapados C. Infrared spectroscopy of aqueous ionic salt solutions at low concentrations: Ion pairing in water. J Chem Phys [Internet]. 2007 [cited 2017 Oct 20];127:114509. Available from: http://dx.doi.org/10.1063/1.2764485

11. Fayer MD, Moilanen DE, Wong D, Rosenfeld DE, Fenn EE, Park S. Water dynamics in salt solutions studied with ultrafast two-dimensional infrared (2D IR) vibrational echo spectroscopy. Acc Chem Res [Internet]. 2009 [cited 2019 Sep 9];42(9):1210–9. Available from: http://europepmc.org/backend/ptpmcrender.fcgi?accid=PMC2745496&blobtype=pdf

12. Van Der Post ST, Scheidelaar S, Bakker HJ. Femtosecond study of the effects of ions on the reorientation dynamics of water. J Mol Liq. 2012;176:22–8.

13. Giammanco CH, Wong DB, Fayer MD. Water dynamics in divalent and monovalent concentrated salt solutions. J Phys Chem B [Internet]. 2012 [cited 2019 Sep 9];116(46):13781–92. Available from: https://pubs.acs.org/sharingguidelines

14. Wei Q, Zhou D, Bian H. Negligible cation effect on the vibrational relaxation dynamics of water molecules in NaClO4 and LiClO4 aqueous electrolyte solutions. RSC Adv [Internet]. 2017 [cited 2019 Sep 9];7(82):52111–7. Available from: https://pubs.rsc.org/en/content/articlepdf/2017/ra/c7ra08840j

15. Zhang N, Shen Z, Chen C, He G, Hao C. Effect of hydrogen bonding on self-diffusion in methanol/water liquid mixtures: A molecular dynamics simulation study. J Mol Liq [Internet]. 2015 [cited 2018 Nov 13];203:90–7. Available from: http://dx.doi.org/10.1016/j.molliq.2014.12.047

16. Sterpone F, Stirnemann G, Hynes JT, Laage D. Water hydrogen-bond dynamics around amino acids: The key role of hydrophilic hydrogen-bond acceptor groups. J Phys Chem B [Internet]. 2010 [cited 2019 Feb 12];114(5):2083–9. Available from: https://pubs.acs.org/sharingguidelines

17. Stirnemann G, Wernersson E, Jungwirth P, Laage D. Mechanisms of acceleration and retardation of water dynamics by ions. J Am Chem Soc [Internet]. 2013 [cited 2019 Sep 9];135(32):11824–31. Available from: https://pubs.acs.org/sharingguidelines

18. Galamba N. On the effects of temperature, pressure, and dissolved salts on the hydrogen-bond network of water. J Phys Chem B [Internet]. 2013 [cited 2019 Sep 9];117(2):589–601. Available from: https://pubs.acs.org/sharingguidelines

19. Baul U, Vemparala S. Ion hydration and associated defects in hydrogen bond network of water: Observation of reorientationally slow water molecules beyond first hydration shell in aqueous solutions of MgCl2. Phys Rev E - Stat Nonlinear, Soft Matter Phys [Internet]. 2015 [cited 2019 Sep 9];91(1):12114. Available from: https://journals.aps.org/pre/pdf/10.1103/PhysRevE.91.012114

20. Nieszporek K, Podkościelny P, Nieszporek J. Transitional hydrogen bonds in aqueous perchlorate solution. Phys Chem Chem Phys [Internet]. 2016 [cited 2019 Sep 9];18(8):5957–63. Available from: www.rsc.org/pccp

21. Shimizu S, Matubayasi N. Ion hydration: Linking self-diffusion and reorientational motion to water structure. Phys Chem Chem Phys [Internet]. 2018 [cited 2019 Sep 9];20(8):5909–17. Available from: https://pubs.rsc.org/en/content/articlepdf/2018/cp/c7cp07309g

22. Laage D, Stirnemann G. Effect of Ions on Water Dynamics in Dilute and Concentrated Aqueous Salt Solutions. J Phys Chem B [Internet]. 2019 [cited 2019 Sep 9];123(15):3312–24. Available from: https://pubs.acs.org/sharingguidelines

23. Kim JS, Wu Z, Morrow AR, Yethiraj A, Yethiraj A. Self-diffusion and viscosity in electrolyte solutions. J Phys Chem B [Internet]. 2012 [cited 2017 Oct 10];116(39):12007–13. Available from: http://pubs.acs.org/doi/pdf/10.1021/jp306847t

24. Pestova ON, Kostikov YP, Khripun MK. X-ray phase analysis of structure of water-salt systems: NaCl-H2O and KCl-H2O. Russ J Appl Chem [Internet]. 2004 [cited 2017 Oct 11];77(7):1066–9. Available from: https://0-link-springer-com.wam.leeds.ac.uk/content/pdf/10.1023%252FB%253ARJAC.0000044149.90755.69.pdf

25. Collins KD, Neilson GW, Enderby JE. Ions in water: Characterizing the forces that control chemical processes and biological structure [Internet]. Vol. 128, Biophysical Chemistry. 2007 [cited 2017 Nov 1]. p. 95–104. Available from: https://ac.els-cdn.com/S0301462207000786/1-s2.0-S0301462207000786-main.pdf?_tid=679d3428-bf05-11e7-a603-00000aacb35e&acdnat=1509541739_f05d30da2158475cfcfe8b8fdd763fd1

26. Winkel K, Seidl M, Loerting T, Bove LE, Imberti S, Molinero V, et al. Structural study of low concentration LiCl aqueous solutions in the liquid, supercooled, and hyperquenched glassy states. J Chem Phys [Internet]. 2011 [cited 2017 Oct 10];134(2):024515. Available from: http://homepage.uibk.ac.at/~c724117/publications/winkel11-jcp.pdf

27. Mancinelli R, Botti A, Bruni F, Ricci MA, Soper AK. Perturbation of water structure due to monovalent ions in solution. Phys Chem Chem Phys [Internet]. 2007 [cited 2017 Oct 10];9(23):2959–67. Available from: http://0-pubs.rsc.org.wam.leeds.ac.uk/en/content/articlepdf/2007/cp/b701855j

28. Mancinelli R, Botti A, Bruni F, Ricci MA, Soper AK. Hydration of sodium, potassium, and chloride ions in solution and the concept of structure maker/breaker. J Phys Chem B [Internet]. 2007 [cited 2017 Oct 10];111(48):13570–7. Available from: http://pubs.acs.org/doi/pdf/10.1021/jp075913v

29. Holzmann J, Ludwig R, Geiger A, Paschek D. Pressure and salt effects in simulated water: Two sides of the same coin? Angew Chemie - Int Ed. 2007;46(46):8907–11.

30. Lenton S, Rhys NH, Towey JJ, Soper AK, Dougan L. Highly compressed water structure observed in a perchlorate aqueous solution. Nat Commun [Internet]. 2017 [cited 2017 Nov 30];8(1):1–5. Available from: https://www.nature.com/articles/s41467-017-01039-9.pdf

31. Mancinelli R, Sodo A, Bruni F, Ricci MA, Soper AK. Influence of concentration and anion size on hydration of H+ ions and water structure. J Phys Chem B [Internet]. 2009 [cited 2017 Oct 10];113(13):4075–81. Available from: http://0-pubs.acs.org.wam.leeds.ac.uk/doi/pdf/10.1021/jp805220j

32. Lenton S, Rhys NH, Towey JJ, Soper AK, Dougan L. Temperature Dependent Segregation in Alcohol-Water Binary Mixtures Is Driven by Water Clustering. Journal of Physical Chemistry B [Internet]. 2018 [cited 2018 Oct 9];7884–94. Available from: https://pubs.acs.org/doi/pdf/10.1021/acs.jpcb.8b03543

33. Soper AK, Dougan L, Crain J, Finney JL. Excess entropy in alcohol-water solutions: A simple clustering explanation. J Phys Chem B [Internet]. 2006 [cited 2018 Nov 28];110(8):3472–6. Available from: https://pubs.acs.org/sharingguidelines

34. Daly L, Lee MR, Piazolo S, Griffin S, Bazargan M, Campanale F, et al. Boom boom pow: Shock-facilitated aqueous alteration and evidence for two shock events in the Martian nakhlite meteorites. Sci Adv [Internet]. 2019 [cited 2019 Sep 23];5(9):eaaw5549. Available from: http://advances.sciencemag.org/

35. Orosei R, Lauro SE, Pettinelli E, Cicchetti A, Coradini M, Cosciotti B, et al. Radar evidence of subglacial liquid water on Mars. Science (80-) [Internet]. 2018 [cited 2018 Oct 9];361(6401):490–3. Available from: http://science.sciencemag.org/

36. Marion GM, Catling DC, Zahnle KJ, Claire MW. Modeling aqueous perchlorate chemistries with applications to Mars. Icarus [Internet]. 2010 [cited 2018 Jun 4];207(2):675–85. Available from: http://faculty.washington.edu/dcatling/Marion2010_PerchlorateFREZCHEM.pdf

37. Chevrier VF, Hanley J, Altheide TS. Stability of perchlorate hydrates and their liquid solutions at the Phoenix landing site, mars. Geophys Res Lett [Internet]. 2009 [cited 2018 Oct 8];36(10). Available from: https://agupubs.onlinelibrary.wiley.com/doi/pdf/10.1029/2009GL037497

38. Siegert MJ, Priscu JC, Alekhina IA, Wadham JL, Berry Lyons W. Antarctic subglacial lake exploration: First results and future plans. Philos Trans R Soc A Math Phys Eng Sci [Internet]. 2016 [cited 2018 Nov 15];374(2059):20140466. Available from: http://dx.doi.org/10.1098/rsta.2014.0466

39. Christner BC, Priscu JC, Achberger AM, Barbante C, Carter SP, Christianson K, et al. A microbial ecosystem beneath the West Antarctic ice sheet. Nature [Internet]. 2014 [cited 2018 Nov 28];512(7514):310–3. Available from: https://www.nature.com/articles/nature13667.pdf

40. Aljohny BO. Halophilic bacterium-A review of new studies. Biosci Biotechnol Res Asia. 2015;12(3):2061–9.

41. Wadsworth J, Cockell CS. Perchlorates on Mars enhance the bacteriocidal effects of UV light. Sci Rep [Internet]. 2017 [cited 2017 Oct 10];7(1):4662. Available from: https://www.nature.com/articles/s41598-017-04910-3.pdf

42. Laurent H, Soper A, Dougan L. Biomolecular self-assembly under extreme Martian mimetic conditions. Mol Phys [Internet]. 2019 [cited 2019 Aug 19];117(22):3398–407. Available from: https://www.tandfonline.com/action/journalInformation?journalCode=tmph20

43. Yancey PH. Organic osmolytes as compatible, metabolic and counteracting cytoprotectants in high

osmolarity and other stresses [Internet]. Vol. 208, Journal of Experimental Biology. 2005 [cited 2019 Sep 24]. p. 2819–30. Available from: https://jeb.biologists.org/content/jexbio/208/15/2819.full.pdf

44. Yancey PH, Gerringer ME, Drazen JC, Rowden AA, Jamieson A. Marine fish may be biochemically constrained from inhabiting the deepest ocean depths. Proc Natl Acad Sci U S A [Internet]. 2014 [cited 2018 Sep 24];111(12):4461–5. Available from: www.pnas.org/cgi/doi/10.1073/pnas.1322003111

45. Meersman F, Bowron D, Soper AK, Koch MHJ. Counteraction of urea by trimethylamine N-oxide is due to direct interaction. Biophys J [Internet]. 2009 [cited 2018 Sep 25];97(9):2559–66. Available from: http://www.bioinformatics.org/

46. Meersman F, Bowron D, Soper AK, Koch MHJ. An X-ray and neutron scattering study of the equilibrium between trimethylamine N-oxide and urea in aqueous solution. Phys Chem Chem Phys [Internet]. 2011 [cited 2018 Jul 31];13(30):13765–71. Available from: www.rsc.org/pccp

47. Sarma R, Paul S. The effect of aqueous solutions of trimethylamine-N-oxide on pressure induced modifications of hydrophobic interactions. J Chem Phys [Internet]. 2012 [cited 2018 Sep 25];137:094502. Available from: http://aip.scitation.org/toc/jcp/137/9

48. Imoto S, Forbert H, Marx D. Water structure and solvation of osmolytes at high hydrstatic pressure: pure water and TMAO solutions at 10 kbar versus 1 bar. Phys Chem Chem Phys [Internet]. 2015 [cited 2018 Sep 25];17:24224. Available from: www.rsc.org/pccp

49. Sasaki Y, Horikawa Y, Tokushima T, Okada K, Oura M, Aida M. Hydration structure of trimethylamine N-oxide in aqueous solutions revealed by soft X-ray emission spectroscopy and chemometric analysis. Phys Chem Chem Phys [Internet]. 2016 [cited 2018 Sep 25];18(39):27648–53. Available from: www.rsc.org/pccp

50. Stirnemann G, Duboué-Dijon E, Laage D. Ab Initio Simulations of Water Dynamics in Aqueous TMAO Solutions: Temperature and Concentration Effects. J Phys Chem B [Internet]. 2017 [cited 2018 Sep 28];121:11189–97. Available from: https://pubs.acs.org/sharingguidelines

51. Sahle CJ, Schroer MA, Juurinen I, Niskanen J. Influence of TMAO and urea on the structure of water studied by inelastic X-ray scattering. Phys Chem Chem Phys [Internet]. 2016 [cited 2018 Sep 25];18(24):16518–26. Available from: www.rsc.org/pccp

52. Pestova ON, Myund LA, Khripun MK, Prigaro A V. Polythermal study of the systems M(ClO4)2-H 2O (M2+ = Mg2+, Ca2+, Sr 2+, Ba2+). Russ J Appl Chem [Internet]. 2005 [cited 2019 Sep 18];78(3):409–13. Available from: https://link.springer.com/content/pdf/10.1007%2Fs11167-005-0306-z.pdf

53. Engineering Toolbox. Density of aqueous solutions of inorganic sodium salts [Internet]. Engineeringtoolbox.com. 2017 [cited 2019 Oct 10]. Available from: https://www.engineeringtoolbox.com/density-aqueous-solution-inorganic-sodium-salt-concentration-d_1957.html

54. Bowron DT, Soper AK, Jones K, Ansell S, Birch S, Norris J, et al. NIMROD: The Near and InterMediate Range Order Diffractometer of the ISIS second target station. Rev Sci Instrum [Internet]. 2010 [cited 2018 Oct 10];81(3):033905. Available from: http://aip.scitation.org/toc/rsi/81/3

55. Soper AK. Inelasticity corrections for time-of-flight and fixed wavelength neutron diffraction experiments. Mol Phys [Internet]. 2009 [cited 2019 Oct 31];107(16):1667–84. Available from: https://www.tandfonline.com/action/journalInformation?journalCode=tmph20

56. Soper AK. Partial structure factors from disordered materials diffraction data: An approach using empirical potential structure refinement. Phys Rev B [Internet]. 2005 [cited 2017 Oct 10];72(10):104204. Available from: https://0-journals-aps-org.wam.leeds.ac.uk/prb/pdf/10.1103/PhysRevB.72.104204

57. Soper AK. Tests of the empirical potential structure refinement method and a new method of application to neutron diffraction data on water. Mol Phys [Internet]. 2001 [cited 2018 Oct 9];99(17):1503–16.

Available from: https://www.tandfonline.com/doi/pdf/10.1080/00268970110056889?needAccess=true

58. Soper AK. Empirical potential Monte Carlo simulation of fluid structure. Chem Phys [Internet]. 1996 [cited 2018 Oct 9];202(2–3):295–306. Available from: https://ac.els-cdn.com/0301010495003576/1-s2.0-0301010495003576-main.pdf?_tid=f8b5a339-13e8-48c8-ad3b-b17e22492d16&acdnat=1539089630_9fffd3c88984bc37bf82741ed2f00e02

59. Hölzl C, Kibies P, Imoto S, Frach R, Suladze S, Winter R, et al. Design principles for high-pressure force fields: Aqueous TMAO solutions from ambient to kilobar pressures. J Chem Phys [Internet]. 2016 [cited 2020 Jan 8];144(14):144104. Available from: https://doi.org/10.1063/1.4944991

60. Usui K, Hunger J, Sulpizi M, Ohto T, Bonn M, Nagata Y. Ab Initio Liquid Water Dynamics in Aqueous TMAO Solution. J Phys Chem B [Internet]. 2015 [cited 2020 Jan 8];119(33):10597–606. Available from: https://pubs.acs.org/sharingguidelines

61. Khan A. A Liquid Water Model: Density Variation from Supercooled to Superheated States, Prediction of H-Bonds, and Temperature Limits. J Phys Chem B [Internet]. 2000 [cited 2018 Nov 13];104(47):11268–74. Available from: https://pubs.acs.org/sharingguidelines

62. Kumar R, Schmidt JR, Skinner JL. Hydrogen bonding definitions and dynamics in liquid water. J Chem Phys [Internet]. 2007 [cited 2018 Nov 13];126(20):204107. Available from: http://aip.scitation.org/toc/jcp/126/20

63. Matsumoto M. Relevance of hydrogen bond definitions in liquid water. J Chem Phys [Internet]. 2007 [cited 2018 Nov 13];126(5):054503. Available from: http://jcp.aip.org/jcp/copyright.jsp

64. Swiatla-Wojcik D. Evaluation of the criteria of hydrogen bonding in highly associated liquids. Chem Phys [Internet]. 2007 [cited 2018 Nov 13];342(1–3):260–6. Available from: www.elsevier.com/locate/chemphys

65. Bandyopadhyay D, Mohan S, Ghosh SK, Choudhury N. Correlation of structural order, anomalous density, and hydrogen bonding network of liquid water. J Phys Chem B [Internet]. 2013 [cited 2018 Nov 13];117(29):8831–43. Available from: https://pubs.acs.org/sharingguidelines

66. Prada-Gracia D, Shevchuk R, Rao F. The quest for self-consistency in hydrogen bond definitions. J Chem Phys [Internet]. 2013 [cited 2018 Nov 13];139(8):084501. Available from: http://aip.scitation.org/toc/jcp/139/8

67. Ozkanlar A, Zhou T, Clark AE. Towards a unified description of the hydrogen bond network of liquid water: A dynamics based approach. J Chem Phys [Internet]. 2014 [cited 2018 Nov 13];141(21):214107. Available from: http://aip.scitation.org/toc/jcp/141/21

68. Auer BM, Skinner JL. Water: Hydrogen bonding and vibrational spectroscopy, in the bulk liquid and at the liquid/vapor interface. Chem Phys Lett [Internet]. 2009 [cited 2018 Nov 13];470(1–3):13–20. Available from: https://ac.els-cdn.com/S000926140900030X/1-s2.0-S000926140900030X-main.pdf?_tid=95611c54-97ad-4f0f-a6da-0faea11393a9&acdnat=1542126555_6b2d28a8e8561993063219f0913a5cd4

69. OriginLab. 2D Kernel Density. Origin User Guide. 2018.

70. Ohto T, Hunger J, Backus EHG, Mizukami W, Bonn M, Nagata Y. Trimethylamine-N-oxide: Its hydration structure, surface activity, and biological function, viewed by vibrational spectroscopy and molecular dynamics simulations [Internet]. Vol. 19, Physical Chemistry Chemical Physics. 2017 [cited 2019 Feb 5]. p. 6909–20. Available from: https://pubs.rsc.org/en/content/articlepdf/2017/cp/c6cp07284d

71. Henchman RH, Cockram SJ. Water's non-tetrahedral side. Faraday Discuss [Internet]. 2013 [cited 2018 Nov 13];167:529–50. Available from: https://pubs.rsc.org/en/content/articlepdf/2013/fd/c3fd00080j

72. Markovitch O, Agmon N. Structure and energetics of the hydronium hydration shells. J Phys Chem A [Internet]. 2007 [cited 2020 Jan 8];111(12):2253–6. Available from: http://pubs.acs.org.

73. Sapir L, Harries D. Revisiting Hydrogen Bond Thermodynamics in Molecular Simulations. J Chem Theory Comput [Internet]. 2017 [cited 2020 Jan 8];13(6):2851–7. Available from: https://pubs.acs.org/sharingguidelines

74. Auton M, Holthauzen LMF, Bolen DW. Anatomy of energetic changes accompanying urea-induced protein denaturation. Proc Natl Acad Sci U S A [Internet]. 2007 [cited 2020 Jan 14];104(39):15317–22. Available from: www.pnas.org/cgi/content/full/

75. Rossky PJ. Protein denaturation by urea: Slash and bond. Proc Natl Acad Sci [Internet]. 2008 Nov 4 [cited 2020 Jan 14];105(44):16825–6. Available from: www.pnas.orgcgidoi10.1073pnas.0809224105

76. Hua L, Zhou R, Thirumalai C D, Berne BJ. Urea denaturation by stronger dispersion interactions with proteins than water implies a 2-stage unfolding. Proc Natl Acad Sci U S A [Internet]. 2008 [cited 2020 Jan 14];105(44):16928–33. Available from: www.pnas.orgcgidoi10.1073pnas.0808427105

77. Canchi DR, Garciá AE. Backbone and side-chain contributions in protein denaturation by urea. Biophys J. 2011 Mar 16;100(6):1526–33.

78. Rose GD, Fleming PJ, Banavar JR, Maritan A. A backbone-based theory of protein folding. Proc Natl Acad Sci U S A [Internet]. 2006 [cited 2020 Jan 14];103(45):16623–33. Available from: www.rcsb.org

79. Canchi DR, Jayasimha P, Rau DC, Makhatadze GI, Garciá AE. Thermodynamics of Hydrophobic Amino Acids in Solution: ACombined Experimental−Computational Study. J Phys Chem B. 2012;116:12095–104.

80. Canchi DR, García AE. Cosolvent Effects on Protein Stability. Annu Rev Phys Chem [Internet]. 2013 [cited 2019 May 13];64(1):273–93. Available from: www.annualreviews.org

81. Liao YT, Manson AC, DeLyser MR, Noid WG, Cremer PS. Trimethylamine N-oxide stabilizes proteins via a distinct mechanism compared with betaine and glycine. Proc Natl Acad Sci U S A. 2017;114(10):2479–84.

82. Mondal J, Halverson D, Li ITS, Stirnemann G, Walker GC, Berne BJ. How osmolytes influence hydrophobic polymer conformations: A unified view from experiment and theory. Proc Natl Acad Sci U S A. 2015 Jul 28;112(30):9270–5.

83. Paul S, Patey GN. Structure and interaction in aqueous urea - Trimethylamine-N-oxide solutions. J Am Chem Soc [Internet]. 2007 [cited 2020 Jan 14];129(14):4476–82. Available from: https://pubs.acs.org/sharingguidelines

84. Yang Y, Mu Y, Li W. Microscopic significance of hydrophobic residues in the protein-stabilizing effect of trimethylamine: N -oxide (TMAO). Phys Chem Chem Phys [Internet]. 2016 [cited 2020 Jan 14];18(32):22081–8. Available from: www.rsc.org/pccp

85. Kokubo H, Hu CY, Pettitt BM. Peptide conformational preferences in osmolyte solutions: Transfer free energies of decaalanine. J Am Chem Soc [Internet]. 2011 [cited 2020 Jan 14];133(6):1849–58. Available from: https://pubs.acs.org/sharingguidelines

86. Smolin N, Voloshin VP, Anikeenko A V, Geiger A, Winter R, Medvedev NN. TMAO and urea in the hydration shell of the protein SNase. Phys Chem Chem Phys [Internet]. 2017 [cited 2020 Jan 14];19(9):6345–57. Available from: www.rsc.org/pccp

87. Ganguly P, Boserman P, Van Der Vegt NFA, Shea JE. Trimethylamine N-oxide Counteracts Urea Denaturation by Inhibiting Protein-Urea Preferential Interaction. J Am Chem Soc [Internet]. 2018 [cited 2019 Apr 17];140(1):483–92. Available from: https://pubs.acs.org/sharingguidelines

88. Chand A, Chowdhuri S. A comparative study of hydrogen bonding structure and dynamics in aqueous urea solution of amides with varying hydrophobicity: Effect of addition of trimethylamine N-oxide (TMAO). J Mol Liq [Internet]. 2017;242:70–81. Available from: http://dx.doi.org/10.1016/j.molliq.2017.06.121